ELSEVIER

7 October 1994

Chemical Physics Letters 228 (1994) 333–340

CHEMICAL PHYSICS LETTERS

Direct and complex-forming collisions in a collinear model for the barrierless proton transfer reaction $CH_3OH + {}^-OCH_3 \rightarrow CH_3O^- + HOCH_3$

Robert J. Hinde [1], Gregory S. Ezra

Baker Laboratory, Department of Chemistry, Cornell University, Ithaca, NY 14853-1301, USA

Received 21 April 1994; in final form 21 July 1994

Abstract

A simplified collinear model for the title reaction is studied using classical trajectory methods. By treating the methoxy groups as united atoms, we reduce the reaction to a three-body heavy–light–heavy system. At low collision energies, both long-lived, complex-forming collisions and 'direct' collisions are observed. The reaction probability for direct collisions is considerably lower than the statistical value 0.5 found for complex trajectories. The observed behavior is analyzed in terms of the phase space structure of the collinear heavy–light–heavy system.

1. Introduction

Identity alcohol/alkoxide proton transfer reactions,

$$ROH + {}^-OR \rightarrow RO^- + HOR\,, \qquad (1)$$

play important roles as reference points, or 'anchors', in measurements of relative gas-phase alcohol acidities and of gas-phase hydrogen bond strengths [1]. This has motivated both several investigations [2–6] of the structure, energetics, and thermodynamics of ion–molecule complexes of the form $[RO...H...OR]^-$ and some recent flowing–afterglow [7] and ion cyclotron resonance [8] studies of the kinetics of reactions (1).

One surprising result of these kinetic studies is that *barrierless* identity alcohol/alkoxide proton transfer reactions proceed at rates substantially below that expected on the basis of the kinetic scheme

$$ROH + {}^-OR \underset{k_d}{\overset{k_a}{\rightleftharpoons}} [RO...H...OR]^- \xrightarrow{k_p} RO^- + HOR\,. \qquad (2)$$

Here, k_a is the rate of formation of ion–molecule complexes, k_d the rate of dissociation of complexes back to reactants, and k_p the rate of dissociation to yield products. In the statistical limit, one-half of all complex-forming collisions will lead to proton transfer, i.e. $k_d = k_p$. The rate for barrierless $ROH + {}^-OR$ proton transfer reactions is then 50% of the complex formation rate k_a, which is usually assumed to be equal to the theoretical [9] ion–dipole collision rate k_{coll} (cf. however, Refs. [10,11]).

Barlow et al. [7], however, find that the efficiency of the methanol/methoxide proton transfer reaction ($R = CH_3$), defined as the ratio $\eta = k_{exp}/k_{coll}$ of the observed rate to the theoretical collision rate, is only about 35%. Dodd et al. [8] also report that this re-

[1] Present address: Department of Chemistry, University of Tennessee, Knoxville, TN 37966, USA.

SSDI 0009-2614(94)00953-8

action is somewhat sluggish, with an efficiency of $\eta=0.26$. To account for the observed rate using RRKM theory [8], it is necessary to assume a sizable energetic barrier to proton transfer. Such a barrier is inconsistent with quantum-mechanical calculations of the $CH_3OH+{}^-OCH_3$ potential surface [2,3,5], which all predict a relatively small barrier.

In an attempt to understand the origin of this reaction's unusually low efficiency, Lim and Brauman [12] have modeled $CH_3OH+{}^-OCH_3$ collisions using quasiclassical trajectory (QCT) methods, treating the methoxy groups as united atoms and using a simple model potential surface with no energetic barrier along the reaction coordinate. They conclude that the dynamics of the model reaction are governed by *two* transition states. The first transition state encountered by the reactants is the familiar one corresponding to passage over the centrifugal barrier arising from orbital motion of the two fragments. The second transition state, termed a 'rotational locking transition state' (RLTS) by Lim and Brauman, is associated with conversion of reactant rotation into bending vibrations as the reactants form a collision complex. Lim and Brauman suggest that passage through the RLTS is the rate-determining step in their model reaction (see also Ref. [13]).

The existence of the RLTS may help explain the unusually low efficiency observed for $CH_3OH+{}^-OCH_3$ collisions in ICR experiments. The definition of η given above assumes that passage over the generalized centrifugal barrier is the only transition state in the reaction; however, if there is a second, inner transition state, it may turn back some trajectories before they reach the region of phase space in which proton transfer occurs. The net effect will be that the denominator of η is too large, as not every trajectory which forms a collision complex (by surmounting the centrifugal barrier) can potentially lead to proton transfer. Hence η as defined above may underestimate the intrinsic efficiency of thermoneutral proton transfer reactions. Moreover, the kinetic model outlined in Eq. (2) fails to account for the role of direct (non-complex-forming) collisions, whether reactive or nonreactive.

We have recently re-examined [14] the Lim and Brauman model for methanol/methoxide collisions with the aim of providing a more precise characterization of the RLTS. In this Letter, however, we examine a *collinear* three-body model methanol/methoxide reaction, $X+HX\rightarrow XH+X$ (here X represents a methoxy group). Restricting the reactants to collinear orientations explicitly eliminates any effects of reactant rotational motion, in the form of either diatomic rotation or orbital angular momentum, and hence allows us to analyze the reaction dynamics in the absence of RLTS effects.

Two types of collisions are observed at thermal energies: long-lived collision complexes and 'direct' collisions (those which do not form a long-lived complex). Both types of collisions may lead to proton transfer. While the complexes react with approximately 50% efficiency, the reaction probability for direct trajectories is much lower, leading to an overall reaction probability substantially below 50%. The dynamics of the proton transfer is further elucidated through analysis of the phase space structure of the collinear two degree of freedom system (cf. Refs. [15,16]).

2. Computational methods

In terms of bond coordinates (r_1, r_2), where r_i is the distance from the H atom to X atom i, the Hamiltonian for our system is

$$H=\frac{1}{2\mu}(p_1^2+p_2^2)-\frac{1}{m_H}p_1p_2+V(r_1,r_2,r_{12}), \quad (3)$$

where p_i is the momentum conjugate to r_i, m_H is the proton mass, m_X the mass of the X atom, and the reduced mass $\mu=m_Hm_X/(m_H+m_X)$. The potential surface we use is that denoted $V_{(1)}$ by Lim and Brauman [12], and is a sum of pairwise interactions,

$$V(r_1,r_2,r_{12})=V_{HX}(r_1)+V_{HX}(r_2)+V_{XX}(r_{12}), \quad (4)$$

where r_{12} is the distance between the two X atoms ($r_{12}=r_1+r_2$ for collinear geometries). The individual terms in V are

$$V_{HX}(r)=D_e\{\exp[-\beta(r-r_{eq})]-1\}^2, \quad (5)$$

and

$$V_{XX}(r)=A/r^{12}-B/r^6-C/r^4-D/r^2-D_eh(r), \quad (6)$$

where the switching function $h(r)$ is given by

$$h(r)=0, \quad \text{if } r<r_{sw},$$

$$h(r)=\{\exp[-\beta(r-r_{sw})]-1\}^2, \quad \text{otherwise}. \qquad (7)$$

The values of the parameters defining the potential surface are taken directly from Ref. [12]; we use masses $m_H=1.0079$ amu and $m_X=31.0341$ amu. Fig. 1 shows constant energy contours for the collinear X+HX surface. Note that there is no energetic barrier along the minimum energy pathway for proton transfer between the X atoms; instead, the potential is dominated by a 1.265 eV-deep well at $r_1=r_2=2.186$ a_0. (The potential is zero for HX held at its equilibrium bond length r_{eq} and placed infinitely far away from the remaining X atom.) The switching function used by Lim and Brauman introduces a discontinuity in the second derivatives of the potential along the line $r_{12}=r_{sw}$ shown in Fig. 1a. However, this line is inaccessible to classical trajectories with energy $E<2$ eV, so that the discontinuity is of no consequence at the low collision energies considered here.

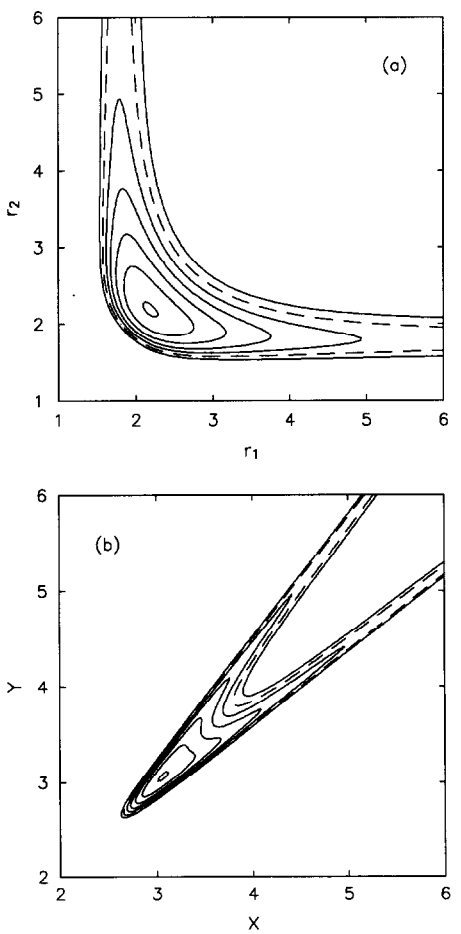

Fig. 1. (a) Potential energy surface $V(r_1, r_2)$ for the collinear X+HX system. Energy contours are drawn every 0.25 eV, with the innermost contour at −1.25 eV; the dashed contour line is at 0.0 eV. Along the dotted line, $r_{12}=r_{sw}$. (b) Skewed and scaled potential surface $V(x, y)$ defined in Section 4. Energy contours are at the same values as in (a). The coordinates r_1, r_2, x, and y are all given in Bohr radii.

Standard QCT methods (described in detail elsewhere [14]) are used to initiate and propagate collinear X+HX($v=0$) trajectories. For each trajectory, we count the number of times the proton is exchanged between the two X atoms, N_X, and the number of inner turning points N_t in the Jacobi coordinate R (the distance from the lone X atom to the HX center of mass). Trajectories for which N_X is odd are reactive, and those with even values of N_X are unreactive. Trajectories with $N_t>1$ are defined as 'complex-forming'; those trajectories with only one inner turning point in R are termed 'direct'.

3. Results

We have studied X+HX($v=0$) collisions at energies ranging from $E=0.2334$ eV to $E=0.3834$ eV; the quasiclassical HX zero-point energy is 0.2234 eV, so these values of E correspond to *collision* energies of $E_{cm}=0.01$–0.16 eV. At each energy, we propagate a batch of trajectories which sample the initial vibrational phase angle ϕ uniformly over the interval $0\leqslant\phi<2\pi$. For $E<0.32$ eV, we use batches of 2000 trajectories; at higher energies, we use batches of 2500 trajectories. More trajectories are used at high energies to insure that at least 1000 trajectories form complexes at each energy. The trajectories are classified according to the above taxonomy; we also record for each trajectory the final vibrational action of the receding HX fragment, I_f.

Contiguous 'bands' of complex-forming, reactive direct, and unreactive direct trajectories are observed at each energy [2]; Fig. 2 depicts these bands at $E=0.2934$ eV. In the ranges of vibrational phase angle ϕ corresponding to direct trajectories (both reactive and unreactive), I_f is a smooth function of ϕ; in

[2] For an early reference to reactivity bands, see Ref. [17].

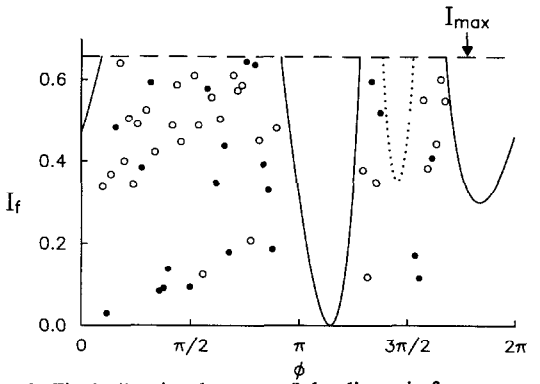

Fig. 2. Final vibrational action of the diatomic fragment as a function of initial vibrational phase ϕ for X+HX collisions at $E=0.2934$ eV. (——) Direct trajectories; (···) reactive direct trajectories; (●) reactive complexes; (○) unreactive complexes, respectively.

the complex-forming bands, however, $I_f(\phi)$ varies erratically in a fashion typical of a system exhibiting chaotic scattering [18]. A similar banded structure is observed at each energy we have studied.

For each batch of trajectories, we compute the fraction P_c of collisions which form complexes and the efficiency η_c of complex-forming trajectories, defined as the fraction of these collisions which result in proton transfer. The efficiency of direct trajectories η_d is defined analogously. Fig. 3 shows how these three quantities vary with total energy E.

The efficiency of complex-forming trajectories η_c is quite close to 50% over the entire energy range shown in Fig. 3. Direct trajectories, however, are very reluctant to react; at the energies considered here, only about 15% of all direct trajectories result in proton transfer. Fig. 3 also indicates that the probability of complex formation P_c declines steadily with energy, from 63% at $E=0.2334$ eV to 41% at $E=0.3834$ eV. The overall efficiency of the reaction is a weighted average over direct and complex-forming trajectories, $\eta=P_c\eta_c+(1-P_c)\eta_d$; because P_c drops off with increasing energy, η falls from 36% at $E=0.2334$ eV to 30% at $E=0.3834$ eV. These results show that the low reaction probability of *direct* X+HX collisions makes the collinear X+HX reaction intrinsically inefficient at thermal energies.

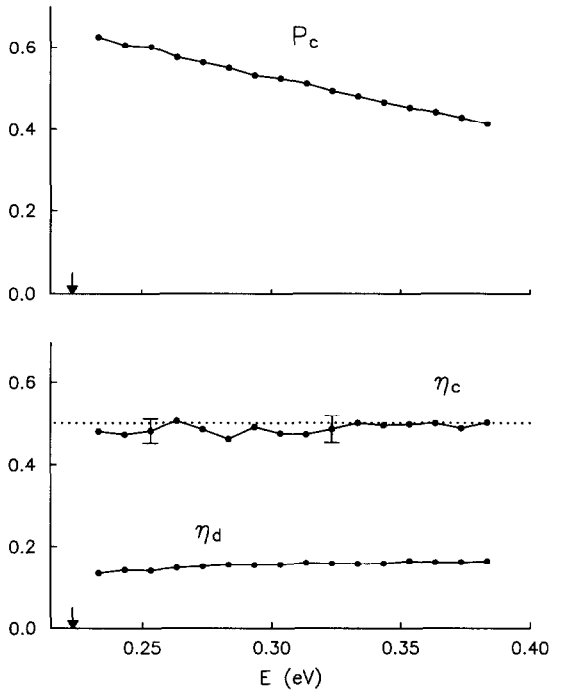

Fig. 3. P_c, η_c, and η_d as functions of total energy E. The arrow at $E=0.2234$ eV indicates the energy of HX in its $v=0$ state. Error bars on η_c are $N^{-1/2}$ estimates, where the number of complex-forming trajectories $N\approx 1000$–1200. No error bars are given for P_c or η_d; this omission is explained in Section 4.

4. Phase-space analysis

Here we define a Poincaré surface of section which uncovers the structures in the collinear X+HX phase space that give rise to the reactivity bands shown in Fig. 2; examination of the collinear phase space also lets us rationalize the extreme inefficiency of direct X+HX trajectories.

The important structures in the phase space of the X+HX system are visualized by defining a Poincaré section based on hyperspherical (polar) coordinates. We first make a transformation from the bond coordinates r_1 and r_2 to new coordinates x and y according to

$$\begin{pmatrix} x \\ y \end{pmatrix} = \begin{pmatrix} a & b \\ b & a \end{pmatrix} \begin{pmatrix} r_1 \\ r_2 \end{pmatrix}, \tag{8}$$

where $ab=\mu/2m_H$ and $a^2+b^2=1$. This change of coordinates transforms the collinear X+HX Hamiltonian to the form

$$H=\left(\frac{1}{2\mu}-\frac{\mu}{2m_H^2}\right)(p_x^2+p_y^2)+V(x,y)\,, \qquad (9)$$

thereby diagonalizing the kinetic energy term while preserving the symmetry of the bond coordinates. Here $V(x, y)$ is the skewed and scaled potential surface shown in Fig. 1b. Hyperspherical coordinates are then defined according to

$$\rho=(x^2+y^2)^{1/2},\quad \theta=\tan^{-1}(y/x)\,. \qquad (10)$$

Hyperspherical coordinates are often used in dynamical studies of HLH systems [19–21] because motion along the ρ coordinate corresponds roughly to motion of the two heavy atoms, while motion along θ corresponds roughly to the antisymmetric-stretch-like vibration of the light particle. We therefore choose the sectioning condition at energy E,

$$p_\rho=0;\quad \mathrm{d}p_\rho/\mathrm{d}t>0;$$
$$\text{and}\ \rho<\rho_{\max}(E)\,, \qquad (11)$$

where p_ρ is the momentum canonically conjugate to ρ and $\rho_{\max}(E)$ is the value of ρ at the outer endpoint of the symmetric stretch line ($\theta=\pi/4$) where the potential $V=E$. Condition (11) is satisfied at those points along a trajectory which are inner turning points in ρ in the deep central well. The HLH nature of the collinear X+HX system causes ρ to be nearly equal to the Jacobi coordinate R, and we find that trajectories have exactly the same number of inner turning points (N_t) in ρ as in R.

Other choices of sectioning condition are of course possible. An alternative section for the present problem is discussed in Ref. [14].

The sectioning condition (11) defines a two-dimensional 'slice' or Poincaré section through the three-dimensional phase space at constant energy E. We record the values of θ and its conjugate momentum p_θ at every intersection of the trajectory with this slice. Fig. 4 shows the resulting portrait of phase space at two energies, $E=0.28$ and 0.35 eV.

The essential features of this figure are understood as follows. There are two key periodic orbits in the collinear X+HX system (one for each distinct channel), in which the X and HX fragments are held infinitely far apart with zero relative translational energy and the HX molecule vibrates with action $I_{\max}(E)$ determined by the total energy E of the system. Each of these periodic orbits has an associated stable manifold [22], consisting of all trajectories which approach the periodic orbit asymptotically in forward time ($t\to\infty$). Similarly, the unstable manifolds consist of all those trajectories which approach

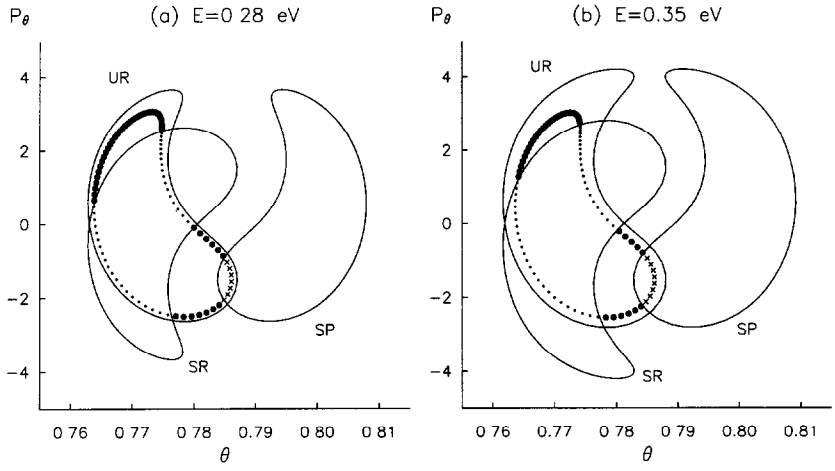

Fig. 4. Phase space structure of the collinear X+HX system at (a) $E=0.28$ eV and (b) $E=0.35$ eV. The stable (unstable) manifold of the asymptotic reactant channel periodic orbit makes its last (first) intersection with the Poincaré section along the curve marked SR (UR). The curve marked SP is the analogous structure for the stable manifold of the product channel asymptotic periodic orbit. Symbols mark the points where a batch of 100 quasiclassical trajectories, entering from the reactant channel and evenly spaced in vibrational phase ϕ, make their first intersection with the surface of section: (×) reactive direct trajectories, (•) unreactive direct trajectories, (●) complex-forming trajectories (both reactive and unreactive).

the periodic orbits asymptotically in reverse time ($t \to -\infty$).

A trajectory with energy E can only escape the deep potential well by moving out along one of the channels of the potential surface to an asymptotic HX vibrational state at $R=\infty$ with action $I_f < I_{max}(E)$. Trajectories which have asymptotic HX actions $I_f > I_{max}(E)$ are ultimately turned back by the long-range ion–dipole potential because they have insufficient relative translational energy to escape. The stable manifolds of the periodic orbits at infinity therefore separate outgoing trajectories that escape as $t \to \infty$ from those that ultimately return [16,22]. In similar fashion, following trajectories out along the channels in backward time, the unstable manifolds of the asymptotic periodic orbits separate those trajectories that escape as $t \to -\infty$ from those that return.

From Fig. 4, we see that trajectories entering the well from the reactant channel make their first intersection with the Poincaré section inside the region marked UR, whose boundary is formed by the unstable manifold of the reactant channel periodic orbit; in order to enter the well, a trajectory must therefore be inside the 'cylinder' formed by the unstable manifold of the asymptotic reactant periodic orbit [23].

Trajectories segregate themselves into reactivity bands as illustrated in Fig. 2. Direct trajectories are those whose first intersection with the Poincaré section falls inside boundaries formed by both a stable and an unstable manifold, while complex-forming trajectories make their first appearance on the surface of section outside either of the regions bounded by the stable manifolds.

This is easily understood. The two areas enclosed by the stable manifolds of the reactant and product asymptotic periodic orbits (the tadpole-shaped areas denoted SR and SP in Fig. 4) contain trajectories that do not return in forward time. These trajectories are therefore making their *final* appearance on the Poincaré section and will subsequently leave the deep central well. Thus if a trajectory's first intersection with the Poincaré section falls inside either SR or SP it must simultaneously be making its final appearance on the surface of section, and must therefore be a direct trajectory. Furthermore, if the direct trajectory intersects the Poincaré section inside the SR region, it is destined to leave the well through the reactant channel, and so must be unreactive. Those direct trajectories which make their first (and last) appearance on the surface of section inside SP are reactive, as they exit along a channel different from that in which they entered. In short, the overlap between UR and SR defines the direct unreactive component of phase space, while the overlap between UR and SP defines the direct reactive component (cf. Ref. [15]).

Next we examine the trajectories which form collision complexes, with two or more inner turning points in the well. Because trajectories can exit the well only after landing inside either the SR or SP regions, any trajectory which first intersects the Poincaré section *outside* either of these areas must make at least one more appearance on the surface of section before leaving the well. Each intersection with the Poincaré section represents an inner turning point in the well, so that such a trajectory is by definition complex forming.

Thus the set of all incoming trajectories in the collinear X+HX system (region UR) is partitioned into direct and complex-forming components by intersection with regions SR and SP (Fig. 4). In particular, the reactivity bands shown in Fig. 2 follow directly from the way in which the initial trajectory ensemble intersects regions SR and SP. In addition, we immediately see that the low η_d values observed for this reaction reflect the small size of the overlap between regions UR and SP. Finally, we note that the SR and SP curves cannot touch, as no point in phase space can belong to the stable manifolds of both the reactant and product channel asymptotic periodic orbits. Thus the reactive and unreactive direct bands of trajectories are always separated by complex-forming bands, as seen in Fig. 2.

We now explain the steady decline of P_c seen in Fig. 3 by comparing the two Poincaré sections shown in Fig. 4. As the energy E increases, the regions enclosed by the stable and unstable manifolds grow larger. However, the size of the loop corresponding to the first intersection of the $v=0$ trajectory ensemble with the sectioning plane remains constant, due to conservation of the symplectic area enclosed by the initial ensemble [24]. The net result is that trajectories that are complex-forming at low energies (the solid circles in Fig. 4 with $p_\theta > 0$) become unreactive direct trajectories at higher energies, leading to a fairly

steady decline in P_c as E increases through the energy range shown in Fig. 3.

As a final comment on Fig. 4, we note that the endpoints of the reactivity bands shown in Fig. 2 can be determined with an accuracy comparable to the spacing between trajectories in ϕ. Hence P_c and η_d, which essentially measure the relative widths of particular reactivity bands, are known to accuracy $\mathcal{O}(N^{-1})$, which is much better than the statistical error estimate of $\mathcal{O}(N^{-1/2})$ used for η_c. The P_c and η_d values given in Fig. 3 are accurate to within ± 0.01, so that error bars for these two quantities would be roughly the same size as the symbols used in that figure.

We conclude this section by comparing the behavior of the collinear X+HX reaction with that of two other collinear HLH systems studied recently: (1) the I+HI reaction examined by Skodje and Davis [25], and (2) the Cl^-+HCl reaction studied by Chapman, Ali, and Hynes [26]. Neutral hydrogen transfer reactions such as I+HI were historically the first collinear HLH systems to be studied in detail. One conclusion drawn from these studies is that such reactions typically exhibit vibrational adiabaticity at low collision energies; as a result, the reaction efficiency oscillates quite strongly as a function of collision energy. QCT studies of I+HI [25,27] show clear evidence for both of these phenomena, while neither is seen in the X+HX reaction. Instead, we find that the final vibrational action I_f is spread over the entire energetically allowed range (Fig. 2) and that the reaction efficiency changes rather slowly with energy (Fig. 3).

The deep central well on the X+HX potential surface is responsible for the breakdown of vibrational adiabaticity. The simple, appealing picture that was developed to rationalize the typical behavior of neutral HLH systems [19,27–29] is based on the assumption that the motions of the light and heavy atoms occur on widely separated time scales. This is not the case in X+HX; the heavy atoms accelerate as they fall into the central well, so that heavy and light atom motion occur on roughly the same time scale in that portion of the potential surface where proton transfer takes place. It remains to be seen, however, how useful an adiabatic separation is for understanding rotational dynamics involved in orbiting complex formation.

A similar breakdown of vibrational adiabaticity is observed by Chapman, Ali, and Hynes [26] in their model Cl^-+HCl reaction. The potential surface for this system is qualitatively rather like the one used here, with a deep central well and long-range attractive ion–dipole entrance and exit valleys, and several similarities are seen in the two systems' dynamics. For example, the overall Cl^-+HCl reaction probability depends only weakly on energy. In addition, a substantial fraction of Cl^-+HCl trajectories forms long-lived collision complexes at low collision energies, and the probability of complex formation decreases with increasing energy. Reactivity bands like those seen here are also evident in collinear Cl^-+HCl.

The primary difference between the Cl^-+HCl and X+HX systems is that the efficiency of direct Cl^-+HCl trajectories is substantially higher than 50%; this leads to an overall reaction efficiency of 70%–80% at the energies studied by Chapman, Ali, and Hynes. Without performing a complete phase space analysis of the Cl^-+HCl system, it is difficult to identify the origin of this discrepancy. We have found [14] that η_d depends sensitively on the mass ratio m_H/m_X and on the shape of the repulsive inner wall of the potential well; both of these factors likely play a role in the observed differences between X+HX and Cl^-+HCl.

Finally, Chapman, Ali, and Hynes note that QCT studies can overestimate the extent of vibrational nonadiabaticity in collinear HLH systems; they find that nonadiabatic effects have a negligible effect on the *semiclassical* reaction probability for Cl^-+HCl, indicating that complex formation is unimportant in the quantum dynamics of this reaction. They show, however, that this result cannot be easily generalized to other HLH ion–molecule reactions. Hence it is important to supplement the present work with quantum studies of collinear X+HX in order to determine the quantum mechanical significance of the large P_c values obtained here.

5. Summary and conclusions

We have performed QCT studies of a collinear three-body heavy–light–heavy model for the reaction $CH_3OH + {}^-OCH_3 \rightarrow CH_3O^- + HOCH_3$, using a model barrierless potential surface developed by Lim and Brauman [12]. Bands of long-lived, complex-form-

ing trajectories and direct, single-turning-point trajectories are observed. Trajectories which form collision complexes react with efficiency $\eta_c \approx 0.50$, which is the statistically expected value for a barrierless thermoneutral reaction. Direct trajectories, however, are relatively inefficient at causing proton transfer, with $\eta_d \approx 0.15$. The overall reaction probability is therefore substantially less than 50%. The presence of reactivity bands indirectly reveals some elements of the underlying phase space structure of the collinear system; by explicitly examining the model system's phase space structure through a Poincaré surface of section defined in hyperspherical coordinates, we can understand both the origin of these bands and the reason that most direct trajectories are unreactive.

We are currently extending our studies of the dynamics of the model X+HX proton transfer to planar and three-dimensional collisions, where the effects of rotation must be understood. Because of the presence of the deep X...H...X well, however, several aspects of the collinear dynamics carry over to the higher dimensional systems [14]. In particular, we find that both direct and complex-forming trajectories contribute to proton transfer in planar and three-dimensional collisions, and that direct collisions are relatively inefficient provided that the HX reactant is neither vibrationally nor rotationally excited.

Acknowledgement

RJH thanks Dr. K.M. Atkins for several helpful conversations. RJH is a National Science Foundation Postdoctoral Fellow, supported by grant CHE-9203634. This work was also supported by NSF grant CHE-9101357.

References

[1] G. Caldwell, M.D. Rozeboom, J.P. Kiplinger and J.E. Bartmess, J. Am. Chem. Soc. 106 (1984) 4660.
[2] J.H. Busch and J.R. de la Vega, J. Am. Chem. Soc. 99 (1977) 2397.
[3] D.A. Weil and D.A. Dixon, J. Am. Chem. Soc. 107 (1985) 6859.
[4] C.R. Moylan, J.A. Dodd, C.C. Han and J.I. Brauman, J. Chem. Phys. 86 (1987) 5350.
[5] S. Wolfe, S. Hoz, C.-K. Kim and K. Yang, J. Am. Chem. Soc. 112 (1990) 4186.
[6] G.J.C. Paul and P. Kebarle, J. Phys. Chem. 94 (1990) 5184.
[7] S.E. Barlow, T.T. Dang and V.M. Bierbaum, J. Am. Chem. Soc. 112 (1990) 6832.
[8] J.A. Dodd, S. Baer, C.R. Moylan and J.I. Brauman, J. Am. Chem. Soc. 113 (1991) 5942.
[9] W.J. Chesnavich, T. Su and M.T. Bowers, J. Chem. Phys. 72 (1980) 2641.
[10] W.L. Hase, C.L. Darling and L. Zhu, J. Chem. Phys. 96 (1992) 8295, and references therein.
[11] G. Ramachandran and G.S. Ezra, J. Chem. Phys. 97 (1992) 6322.
[12] K.F. Lim and J.I. Brauman, J. Chem. Phys. 94 (1991) 7164.
[13] K.F. Lim and R.I. Keir, J. Chem. Phys. 97 (1992) 1072.
[14] R.J. Hinde and G.S. Ezra, in preparation.
[15] E. Pollak, in: Theory of chemical reaction dynamics, Vol. 3, ed. M. Baer (CRC Press, Boca Raton, 1985).
[16] M.J. Davis and R.T. Skodje, Advan. Class. Traj. Meth. 1 (1992) 77.
[17] J.S. Wright, K.G. Tan and K.J. Laidler, J. Chem. Phys. 64 (1976) 970.
[18] B. Eckardt, Physica D 33 (1988) 89.
[19] V.K. Babamov and R.A. Marcus, J. Chem. Phys. 74 (1981) 1790.
[20] C.L. Shoemaker, N. AbuSalbi and D.J. Kouri, J. Phys. Chem. 87 (1983) 5389.
[21] D.K. Bondi, J.N.L. Connor, J. Manz and J. Römelt, Mol. Phys. 50 (1983) 467.
[22] S. Wiggins, Introduction to applied nonlinear dynamical systems and chaos (Springer, Berlin, 1990).
[23] A.M. Ozorio de Almeida, N. DeLeon, M. Mehta and C.C. Marston, Physica D 46 (1990) 265.
[24] V.I. Arnold, Mathematical methods of classical mechanics (Springer, Berlin, 1978).
[25] R.T. Skodje and M.J. Davis, J. Chem. Phys. 88 (1988) 2429.
[26] S. Chapman, D.P. Ali and J.T. Hynes, Chem. Phys. 136 (1989) 297.
[27] R.T. Skodje, J. Chem. Phys. 90 (1989) 6193.
[28] C. Hiller, J. Manz, W.H. Miller and J. Römelt, J. Chem. Phys. 78 (1983) 3850.
[29] R.T. Skodje, Ann. Rev. Phys. Chem. 44 (1993) 145.